# Evaluating Platinum-Based Ionic Polymer Metal Composites as Potentiometric Sensors for Dissolved Ozone in Ultrapure Water Systems

*Roman Grimmig,\* Philipp Gillemot, Simon Lindner, Philipp Schmidt, Samuel Stucki, Klaus Günther, Helmut Baltruschat, and Steffen Witzleben*

Monitoring the content of dissolved ozone in purified water is often mandatory to ensure the appropriate levels of disinfection and sanitization. However, quantification bears challenges as colorimetric assays require laborious off-line analysis, while commercially available instruments for electrochemical process analysis are expensive and often lack the possibility for miniaturization and discretionary installation. In this study, potentiometric ionic polymer metal composite (IPMC) sensors for the determination of dissolved ozone in ultrapure water (UPW) systems are presented. Commercially available polymer electrolyte membranes are treated via an impregnation-reduction method to obtain nanostructured platinum layers. By applying 25 different synthesis conditions, layer thicknesses of 2.2 to 12.6 µm are obtained. Supporting radiographic analyses indicate that the platinum concentration of the impregnation solution has the highest influence on the obtained metal loading. The sensor response behavior is explained by a Langmuir pseudo-isotherm model and allows the quantification of dissolved ozone to trace levels of less than 10 µg L$^{-1}$. Additional statistical evaluations show that the expected Pt loading and radiographic blackening levels can be predicted with high accuracy and significance ($R^2_{adj.} > 0.90$, $p < 10^{-10}$) solely from given synthesis conditions.

## 1. Introduction

In the pharmaceutical and semiconductor industry, the use of sanitized ultrapure water is mandatory for the production and preparation of medical products and microprocessors.[1–3] In order to obtain and store water of different quality standards (e.g. *aqua purificata,* water for injection), various disinfection strategies are in use.[4–6] Concerning the production and energy-efficient cold storage of sanitized, pressurized water, electrochemically produced ozone ($O_3$) is the disinfectant of choice.[7,8]

Although the stored water is allowed to contain minimal amounts of dissolved ozone ensuring sterility,[9] the process water should be clear of any oxidizing agents.[2] Consequently, a reliable method to monitor the concentration of dissolved ozone in water is required. However, common reference methods have shown to be rather inconvenient as they are based on sampling and off-line analysis, typically including a wet chemical processing step followed by a spectroscopic[10–12] or titrimetric[13,14] determination. Thus, an on-line method with an electrochemical sensor suitable for aqueous application is desired in order to obtain quick and continuous readings.

Within the past 40 years, different amperometric[15,16] and voltammetric[17–19] sensor systems have become the industry

R. Grimmig, P. Gillemot, P. Schmidt, S. Witzleben
Bonn-Rhein-Sieg University of Applied Sciences Department of Natural Sciences
von-Liebig-Str. 20, 53359 Rheinbach, Germany
E-mail: roman.grimmig@h-brs.de

S. Lindner
Research Centre for Experimental Marine Biology and Biotechnology
Plentzia Marine Station
PiE-UPV/EHU
University of the Basque Country
Plentzia 48620, Spain

S. Stucki
Innovatec Gerätetechnik GmbH
von-Liebig-Str. 6, 53359 Rheinbach, Germany

K. Günther
Institute for Bio- and Geosciences (IBG-2)
Research Centre Jülich
Wilhelm-Johnen-Straße, 52428 Jülich, Germany

H. Baltruschat
Clausius Institute of Physical and Theoretical Chemistry
University of Bonn
Römerstr. 164, 53117 Bonn, Germany

**ADVANCED
SCIENCE NEWS**

www.advancedsciencenews.com

**ADVANCED
MATERIALS
TECHNOLOGIES**

www.advmattechnol.de

standard, leading to commonly used commercial ozone sensors, for example, from the Orbisphere product family as used in previous studies.[9,20] However, miniaturization and the suitability for adaption into an embedded system are limited and add to the setup cost, which is why these devices are often only installed at one spot within water storage systems.

When it comes to compact setups, a widely used type of sensor material is based on polymer electrolyte membranes (PEM) containing catalytic layers of defined metal loading. The required noble metal surface can be obtained using different approaches,[21,22] including the impregnation-reduction technique.[23–25] Therein, Nafion acts as a solid ion exchanger and allows the exchange with metal cations, which are subsequently reduced to their metallic state. Depending on the noble metals and reductants used, the resulting ionic polymer metal composite (IPMC) can be tailored to its specific application.[26,27] Most commonly, these materials find their field of application in the detection of hydrogen peroxide,[28] dissolved and gaseous hydrogen[29–32] as well as gaseous ozone.[15,33–35] However, for the detection of dissolved oxygen species in aqueous media, only a few sensor systems are reported.[36–38]

The influence of preparation parameters of such IPMCs has previously been discussed by Sakthivel et al.,[31] however, this has only been investigated in the context of hydrogen sensors. Furthermore, by determining the surface characteristics of Pt electrodes, correlations between the particle size and the amperometric sensor response were identified. Furthermore, it has been reported that incorporating nanoparticles in the IPMC structure influences the properties of a material in the application as a potentiometric sensor.[39] As the use of a supporting solution during the impregnation-reduction process has been reported, Pt layer formation might be altered by influencing the establishing equilibria within the ion exchange membrane from both sides.[40] Thus, a deeper knowledge of the structural composition is equally desired for the development of highly sensitive potentiometric ozone sensors.

The determination of the metal loading is described in varying quality within the literature, as often enough a thorough, comprehensible analytical procedure is not provided. For IPMC specimens with large dimensions, the loading is commonly determined gravimetrically,[24,41] while for low absolute metal content a digestion in aqua regia followed by ICP OES analysis is favored.[42–44] In addition, the application of image processing after TEM analysis has been successfully evaluated.[40]

This study covers the preparation of platinum-based IPMC sensor materials for the application as potentiometric sensors, suitable for the quantification of aqueous ozone in ultrapure water (UPW). By systematic variation of critical synthesis parameters during the impregnation-reduction process, different sensor materials with varying appearances are obtained. The prepared surfaces are thoroughly characterized regarding their physicochemical properties and evaluated in terms of their ozone-sensing characteristics. From the collected data, structure-property relationships are identified and provide guidelines for the preparation of compact, tailor-made sensors using suitable synthesis conditions.

**Table 1.** Analytical parameters for regression functions of both Pt content as well as dissolved ozone. For each analytical method, the upper limit of quantification (ULOQ), limits of detection (LOD), and quantification (LOQ) as well as the coefficient of determination ($R^2$) are given and show satisfactory values. Additionally, the method precision is given as the coefficient of variation of the procedure ($V_{x0}$).

| Method | Pt | O$_3$ | |
| --- | --- | --- | --- |
| | ICP OES radial configuration | DPD method via VIS spectroscopy with 5 cm cuvette | DPD method via VIS spectroscopy with 1 cm cuvette |
| $\lambda$ / nm | 370.6 | 510.0 | 510.0 |
| ULOQ [mg L$^{-1}$] | 20.0 | 0.12 | 2.4 |
| LOD [µg L$^{-1}$] | 51.3 | 0.9 | 43.1 |
| LOQ [µg L$^{-1}$] | 213.0 | 3.2 | 130.5 |
| $R^2$ | 0.9997 | 0.9998 | 0.9994 |
| $V_{x0}$ [%] | 2.1 | 1.5 | 2.1 |

## 2. Results and Discussion

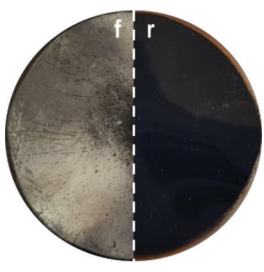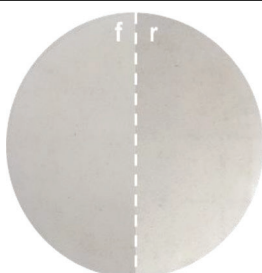### 2.1. Analytical Performance of Spectroscopic Determination Methods

For a thorough characterization of the sensor material, the ability to accurately determine the quantity of Pt deposited per membrane surface area and the concentration of O$_3$ in UPW is central to this study. This is especially true for the quantification of the metal loading as gravimetric determination approaches suffer from poor sensitivity due to the low absolute weight of the noble metal incorporated within the IPMC.

Hence, a more selective and precise spectroscopic determination was chosen for this study. To ensure an exhaustive removal of the metal layer from the IPMC electrode after digestion with aqua regia, the absence of Pt signals from the residual Nafion substrate was confirmed via X-ray fluorescence.

The performed calibrations were described regarding their analytical capabilities, which are given in **Table 1**. LOD and LOQ values were calculated using a calibration approach according to DIN ISO 11843-2:2006-06 and DIN 32645:2008-11.

A wide calibration range from 20.0 mg L$^{-1}$ down to just 213 µg L$^{-1}$ Pt content allows for the analysis of digested samples that originate from both heavily loaded electrode surfaces as well as barely coated IPMC materials. For ozone concentrations, a range from 2.4 mg L$^{-1}$ down to 0.9 µg L$^{-1}$ is suitable to reliably detect traces of dissolved ozone emerging after short periods of electrolysis operation or operational conditions involving low current densities. It must be noted that these analytical limitations can only be reached when the highest grade UPW (18.2 MΩ cm resistivity, total organic carbon ≤ 1 µg L$^{-1}$) is used, as the presence of natural organic matter or other reactive oxygen species may bear additional challenges. The calibration curves for all analytical procedures were fitted to linear functions with coefficients of determination $R^2$ > 0.999 and coefficients of variation less than 2.1 %, stressing the precision and suitability of the chosen methods.

**ADVANCED
SCIENCE NEWS**

www.advancedsciencenews.com

**ADVANCED
MATERIALS
TECHNOLOGIES**

www.advmattechnol.de

**Table 2.** Visual appearance of a representative selection of IPMC sensor materials and their specific synthesis conditions (top view, photomontage). The electrode surface exposed to the impregnation-reduction process (front side, marked "f", pointing upwards during the synthesis) is shown on the left half of the picture, whereas the right half of the picture refers to the rear of the electrode surface which was exposed to the supporting solution (marked "r", pointing downwards).

| Specimen | #10 | #7 | #25 |
|---|---|---|---|
| IPMC appearance | | | |
| Reducing agent | $KBH_4$ | $KBH_4$ | $N_2H_4$ |
| Reductant concentration | 40 mmol $L^{-1}$ | 200 mmol $L^{-1}$ | 25 000 mmol $L^{-1}$ ($\omega = 80$ %) |
| Reduction strategy | $3 \times 20$ min | $1 \times 60$ min | $1 \times 60$ min |
| Pt concentration | 4.5 mmol $L^{-1}$ | 4.5 mmol $L^{-1}$ | 2.0 mmol $L^{-1}$ |
| Supporting solution | | $K_2SO_4$, 13 mmol $L^{-1}$ | |



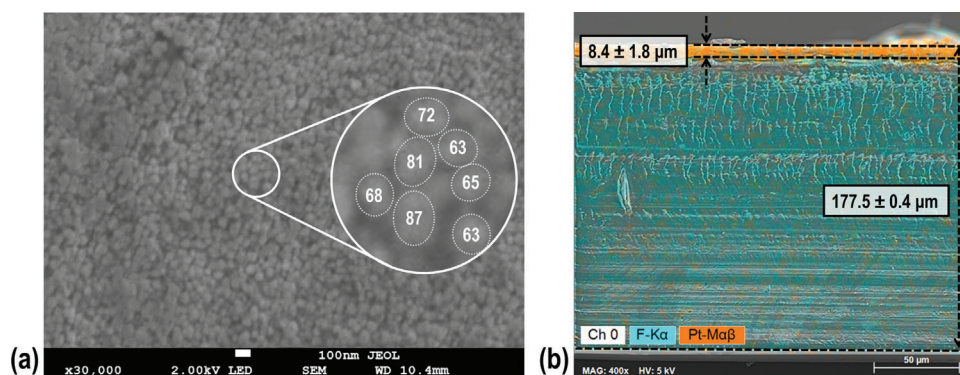**Figure 1.** a) SEM image of the IPMC surface which has undergone a 200 mmol $L^{-1}$ $KBH_4$ reduction step, revealing spherical and elliptical nanoparticles which were measured using digital image processing software (additional 400% digital zoom in the circular segment). Values represent the (longest) diameter of individual nanoparticles. b) For facilitated visual interpretation of the SEM/EDX image of the cross-section of the electrode, characteristic fluorescence energies of fluorine and platinum were colored, representing the bulk Nafion material (turquoise, 178 µm total thickness) and the incorporated surficial Pt layer (orange) with a thickness of ≈8 µm.

## 2.2. Influence of Synthesis Parameters on the Physicochemical Properties of Sensor Material

The synthesis leads to flexible IPMC sensor materials which vary in visual appearance, depending on the synthesis conditions. All sensor materials show substantial staining of the underlying Nafion substrate which ranges from a translucent gray darkening to a solid matte black appearance on both sides and even to a silver-colored, mirror-like front finish (see **Table 2**). The reduced translucence of the sensor materials is accompanied by an increase in the perceived resistance to elastic deformation.

When simply comparing the visual appearance, it becomes apparent that the choice of reducing agent bears a considerable impact. The use of hydrazine ($N_2H_4$) only leads to an extensively stained sensor material which hints at a low Pt loading. Under the given conditions, tetraborohydride acts as a powerful reducing agent[45] and leads to substantially reduced visual transparency, which can be completely blocked at lower reductant concentrations due to the formation of a solid metal deposit on the IPMC surface.

In order to obtain the morphological properties of the synthesized IPMC electrodes, SEM studies were conducted. For an exemplary sensor material, both the surface and cross-section are displayed in **Figure 1**.

By observing the sensor materials at a magnification level of 30 000 in Figure 1a, surficial layers of structured metal deposits become clearly visible. Agglomerates are identified as spherical-shaped Pt nanoparticles via EDX with mean particle sizes ranging between 40 and 90 nm. This is larger than reported for layers obtained under comparable conditions at elevated temperatures[43,46] or from recast Nafion solutions.[47,48]

**ADVANCED
SCIENCE NEWS**

www.advancedsciencenews.com

**ADVANCED
MATERIALS
TECHNOLOGIES**

www.advmattechnol.de

However, this observation is only valid for sensor materials that have undergone a reduction using tetraborohydrides, as hydrazine solutions did not result in electrodes which allowed for the identification of individual Pt particles. Furthermore, for the given dataset, statistically significant smaller particle sizes are measured when using KCl or $K_2SO_4$ electrolytes in contrast to UPW. For all sensor materials, additional cross-sections were prepared and evaluated. EDX analyses revealed that the applied synthesis procedure leads to controlled one-sided precipitation of Pt particles, which can be a valuable feature for an IPMC sensor design. Obtained layer thicknesses are within a range of 2.2 to 12.6 μm, which is in accordance with the results achieved by other researchers[40,49] although even thinner layers have been reported previously, partially using elevated temperatures.[41,50] Electrodes that were prepared with hydrazine as the reducing agent yielded no defined Pt layer that could be identified via SEM/EDX. This is because, in contrast to the anionic borohydride, hydrazine is not subject to Donnan exclusion[51] and can thusly undergo diffuse reduction reactions over the entire cross-section of the IPMC material.

For accurate measurements, the sensor material has to be digested and is consequently destroyed during the quantification process. For that reason, the applicability of radiography as an alternative non-destructive method was evaluated to reliably approximate the Pt loading by determining the radiographic blackening caused by X-ray absorption. This technique makes use of differing material contrasts between the polymer substrate and the incorporated heavy metal atoms.

After the digital reconstruction of the radiographic image, a gray value image is obtained. As within the 8-bit grayscale 256 different shades of gray or black can be differentiated, this leads to a discrimination limit of ≈0.4%. In **Figure 2** the obtained radiographic blackening values are displayed with respect to the elemental content found after digestion and atomic spectroscopy.

The obtained Pt loadings in this study range from 0.01 to 1.52 mg cm$^{-2}$ and comply with the range of sensor materials reported in the literature, which usually exhibit a noble metal loading of 0.1 to 4 mg cm$^{-2}$.[21,41,49,52] Elevated levels of Pt loading in the final product are shown to be obtained primarily by increasing the initial Pt concentration of the impregnation solution. For the given electrodes, a corresponding radiographic blackening from 22.0% to 34.3% was observed. However, it must be noted that any contribution to an increased gray value may also be caused in part by incorporated elements other than Pt due to incomplete restoration of the initial, fully H$^+$-loaded state during the work-up. For Pt loadings in the range of 0 to 0.3 mg cm$^{-2}$, the calculated gray values exhibit considerable deviations, implying comparable analytical limitations as gravimetric approaches.

When all sensor materials are considered, a coefficient of determination $R^2 = 0.725$ for a linear regression model is obtained, which is insufficient for analytical purposes. In contrast, when omitting electrodes with KCl or $K_2SO_4$ electrolytes, an improved $R^2 = 0.876$ can be achieved. This allows for a reasonable, non-destructive estimation of the absolute Pt loading, especially for higher loading values. While previous work on the radiographic determination of heavy metal contents yielded even higher $R^2$ values, these studies have predominantly focused on aqueous matrices, enabling more advanced measuring and quantification
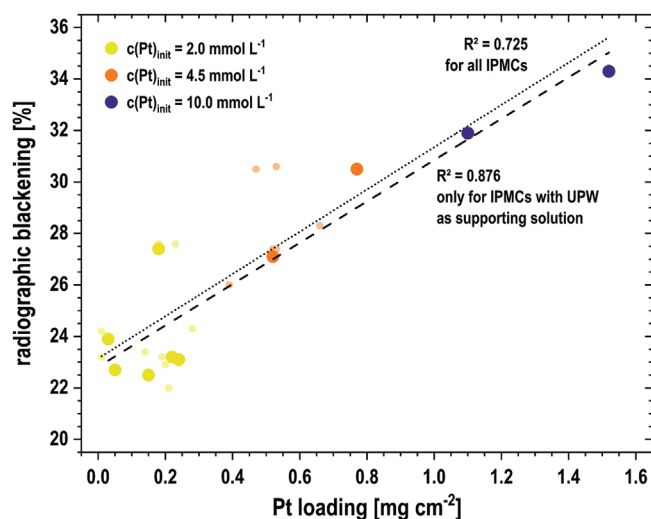


**Figure 2.** Scatter plot of averaged radiographic blackening versus mean Pt loading for individual specimens, determined via digestion and spectroscopic determination. The color scale of the data points correlates with the initial Pt concentration. Smaller data points represent sensor materials prepared with KCl or $K_2SO_4$ electrolytes whereas larger data points show specimens prepared with ultrapure water as supporting solution. Discrete group formation hints at higher Pt concentrations during synthesis also leading to higher elemental content in the final IPMC electrode. Linear trend functions were estimated for all sensor materials (dotted line) as well as only those IPMCs obtained using ultrapure water as a supporting solution (dashed line).

methods.[53,54] Nonetheless, the proposed method may already be sufficient for technical applications (e.g. process and quality control).

A comprehensive overview of the physicochemical parameters obtained for all synthesis conditions is given in **Table 3**. For several specimens, a distinguishable nanostructured Pt layer could not be characterized during SEM analysis and therefore no value is given for layer thickness and/or particle size (denoted n.d.). To ensure highest accuracy for all synthesis conditions, the reported Pt loading values are all obtained from ICP OES measurements.

### 2.3. Evaluation of the Performance of Synthesized IPMC Materials as Potentiometric Electrodes for Ozone Sensing

Prior to a measuring sequence, all synthesized specimens were equilibrated for 24 h with ultrapure water, resulting in a stable voltage baseline ($U_b$) between the IPMC and the IrO$_x$ reference electrodes. A substantial change in voltage is observed within 2 min after exchanging the ultrapure water with ozonated UPW, as dissolved ozone molecules interact with the electrode surface. Once the maximum voltage ($U_{max}$) is reached, it is followed by a slow signal decrease back to the initial voltage $U_b$ over a time period of up to 10 h due to successive ozone decomposition. Exposing the sensor material to solutions with higher content of dissolved ozone leads to a correspondingly increased sensor signal. A stable voltage baseline signal was always re-obtained over the measurement period of about two weeks per specimen, indicating no significant irreversible changes in sensing properties

**ADVANCED
SCIENCE NEWS**

www.advancedsciencenews.com

**ADVANCED
MATERIALS
TECHNOLOGIES**

www.advmattechnol.de

**Table 3.** Comprehensive overview of the physicochemical properties obtained for the 25 sensor materials depending on their respective synthesis conditions. Sensor materials are sorted by their initial Pt impregnation solution concentration, reducing agents, reductant concentration, reduction strategy, and supporting solution. Mean values are given for the Pt loading leached from the electrode, radiographic blackening as well as Pt layer thickness and particle sizes (rounded to the nearest 5 nm).

| # | Synthesis parameters | | | | | Measured physicochemical IPMC properties | | | |
|---|---|---|---|---|---|---|---|---|---|
| | Initial $c(Pt)$ [mmol L$^{-1}$] | Reducing agent | Initial $c(red.)$ [mmol L$^{-1}$] | Reduction strategy | Supporting solution | Pt loading [mg cm$^{-2}$] | Blacke-ning [%] | Layer thickness [µm] | Particle size [nm] |
| 1 | 10.0 | NaBH$_4$ | 200 | 1 × 60 min | UPW | 1.52 | 34.3 | 5.0 | n.d. |
| 2 | 10.0 | NaBH$_4$ | 40 | 3 × 20 min | UPW | 1.10 | 31.9 | 4.5 | 90 |
| 3 | 4.5 | NaBH$_4$ | 200 | 1 × 60 min | KCl | 0.66 | 28.3 | 6.7 | 75 |
| 4 | 4.5 | NaBH$_4$ | 40 | 3 × 20 min | KCl | 0.39 | 26.0 | 10.2 | 55 |
| 5 | 4.5 | KBH$_4$ | 200 | 1 × 60 min | UPW | 0.77 | 30.5 | 8.4 | 65 |
| 6 | 4.5 | KBH$_4$ | 200 | 1 × 60 min | KCl | 0.47 | 30.5 | 7.9 | 45 |
| 7 | 4.5 | KBH$_4$ | 200 | 1 × 60 min | K$_2$SO$_4$ | 0.53 | 30.6 | 5.7 | 65 |
| 8 | 4.5 | KBH$_4$ | 40 | 3 × 20 min | UPW | 0.52 | 27.1 | 4.3 | 70 |
| 9 | 4.5 | KBH$_4$ | 40 | 3 × 20 min | KCl | 0.53 | 27.4 | 12.6 | 50 |
| 10 | 4.5 | KBH$_4$ | 40 | 3 × 20 min | K$_2$SO$_4$ | 0.52 | 27.4 | 2.2 | 75 |
| 11 | 2.0 | NaBH$_4$ | 200 | 1 × 60 min | UPW | 0.24 | 23.1 | 7.5 | n.d. |
| 12 | 2.0 | NaBH$_4$ | 200 | 1 × 60 min | K$_2$SO$_4$ | 0.19 | 23.2 | 5.5 | n.d. |
| 13 | 2.0 | NaBH$_4$ | 200 | 3 × 20 min | UPW | 0.22 | 23.2 | 8.7 | n.d. |
| 14 | 2.0 | NaBH$_4$ | 200 | 3 × 20 min | KCl | 0.20 | 22.9 | 5.5 | 65 |
| 15 | 2.0 | NaBH$_4$ | 200 | 3 × 20 min | K$_2$SO$_4$ | 0.14 | 23.4 | 6.8 | 40 |
| 16 | 2.0 | NaBH$_4$ | 40 | 1 × 60 min | K$_2$SO$_4$ | 0.28 | 24.3 | 4.3 | 55 |
| 17 | 2.0 | NaBH$_4$ | 40 | 3 × 20 min | UPW | 0.15 | 22.5 | 5.7 | 85 |
| 18 | 2.0 | NaBH$_4$ | 40 | 3 × 20 min | K$_2$SO$_4$ | 0.21 | 22.0 | 3.8 | 50 |
| 19 | 2.0 | KBH$_4$ | 200 | 3 × 20 min | UPW | 0.18 | 27.4 | 7.9 | n.d. |
| 20 | 2.0 | KBH$_4$ | 200 | 3 × 20 min | KCl | 0.23 | 27.6 | 7.4 | 70 |
| 21 | 2.0 | KBH$_4$ | 200 | 3 × 20 min | K$_2$SO$_4$ | 0.18 | 27.6 | 10.3 | n.d. |
| 22 | 2.0 | N$_2$H$_4$ | 2000 | 1 × 60 min | UPW | 0.03 | 23.9 | n.d. | 55 |
| 23 | 2.0 | N$_2$H$_4$ | 2000 | 1 × 60 min | KCl | 0.01 | 23.2 | n.d. | n.d. |
| 24 | 2.0 | N$_2$H$_4$ | 25 000 | 1 × 60 min | UPW | 0.05 | 22.7 | n.d. | n.d. |
| 25 | 2.0 | N$_2$H$_4$ | 25 000 | 1 × 60 min | K$_2$SO$_4$ | 0.01 | 24.2 | n.d. | n.d. |

due to, for example, degradation effects and therefore not limiting the reusability of the presented sensor materials. As an example displayed in **Figure 3**a, varying ozone concentrations in a range of 0.07 to 0.83 mg L$^{-1}$ resulted in signal responses from 75 to 200 mV.

In an aqueous solution, dissolved ozone undergoes a complex decomposition mechanism, which is strongly affected by the given reaction conditions. However, there is no univocal model for ozone decay, hence reaction orders ranging from 1 to 2 are discussed in the literature.[55–57] Since the experiments in the present study were performed under atmospheric conditions, all solutions were slightly acidic (pH ≈ 5.5) and ensured that the pH-sensitive IrO$_x$ electrode produced a well-defined reference potential. As first-order kinetics are preferably applied for acidic environments, this approximation was chosen and yielded a fit with $R^2_{adj.} > 0.96$. This enabled us to quantify the mean half-life of the unstable ozone solutions colorimetrically as 80 min, which is in congruence with the findings of previously reviewed studies.[55] Therefore, the concentration at the measured peak maximum

$\beta(O_3)_{t(U_{max})}$ was calculated according to Equation (1) based on the measured initial ozone concentration $\beta(O_3)_{t = 0}$.

$$\beta(O_3) = \beta(O_3)_{t = 0} \cdot e^{-k \cdot t} = \beta(O_3)_{t = 0} \cdot 2^{-\frac{t}{t_{1/2}}}$$

$$\text{with } t_{1/2} = \frac{\ln(2)}{k} \tag{1}$$

The measured voltage differences ($\Delta U_{max} = U_{max} - U_b$) for these potentiometric sensors form response curves that are a function of the ozone concentration at peak maximum (Figure 3b). As the experimental setup only allows the observation of transient voltage signals, a true adsorption equilibrium cannot be established due to successive ozone decay. Furthermore, ozone shows reactive adsorption, as only atomic oxygen forms a chemisorption layer on the Pt surface.[58] Since ozone molecules are not re-formed during the subsequent desorption, an equilibrium state cannot be achieved either. Instead, a slow, kinetically inhibited desorption of surface-bound oxygen atoms occurs,
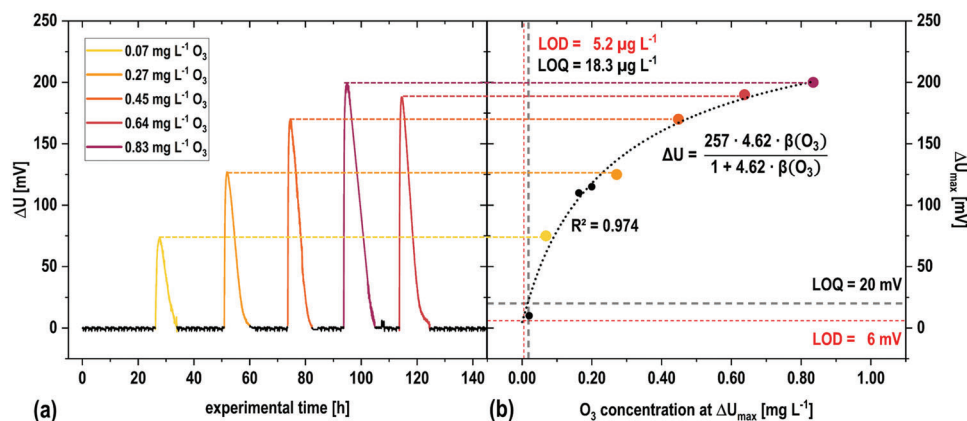
**ADVANCED
SCIENCE NEWS**

www.advancedsciencenews.com

**ADVANCED
MATERIALS
TECHNOLOGIES**

www.advmattechnol.de

**Figure 3.** a) Baseline-corrected potential curve for an exemplary representative sensor (#18). Colors indicate the sensor response to ozonated water of different concentrations. Higher ozone concentrations are linked to higher sensor voltages. Over the course of several hours, the signal drops back to the same, stable baseline level due to successive ozone decomposition even when a lower ozone concentration follows the measurement of a higher concentrated solution, indicating the absence of a 'carryover effect'. b) Sensor response as a function of the calculated ozone concentration at peak maximum for sensor #18. Colored dots are directly derived from (a) whereas black dots represent additional data points obtained for this sensor. The sensor response curve is satisfactorily described by a Langmuir pseudo-isotherm. Additionally, the analytical limits for detection (light red dashed lines) and quantification (light gray dashed lines) are shown in terms of the electrical signal as well as ozone concentration.

possibly as $O_2$ due to recombination.[59] Therefore, the obtained response curves are only described by pseudo-isotherms.

In order to characterize the occurring adsorption behavior, the Freundlich[60] and Langmuir[61] models were fitted to the experimental data and compared by Akaike's information criterion ($AIC_c$) for small sample sizes (Equation (2)).[62,63] Herein, $N$ is the number of data points per sensor, $K$ is the number of parameters within the regression model, and $RSS$ is the residual sum of squares.

$$AIC_c = N \cdot \ln\left(\frac{RSS}{N}\right) + 2K + \frac{2K^2 + 2K}{N - K - 1} \quad (2)$$

As for the vast majority of sensors lower $AIC_c$ values are obtained for the Langmuir pseudo-isotherm, this model seems more suitable to explain the sensor response curves and suggests that only a monolayer of adsorbates is formed on the Pt surface. To further account for possible deviations from a strict pseudo-Langmuir behavior, both the Redlich–Petersen[64] and Sips[65,66] isotherms are also considered suitable regression models.[67] However, the gain in the goodness of fit does not lead to an overall decrease in $AIC_c$ values (see **Table 4**) and therefore does not justify the introduction of a third regression parameter, also preventing overfitting. Hence, the Langmuir pseudo-isotherm model (Equation (3)) is selected for subsequent sensor characterization.

$$\Delta U_{max}\left(\beta(O_3)_{t(U_{max})}\right) = f \cdot q_e = \frac{q_{max} \cdot K_L \cdot \beta(O_3)_{t(U_{max})}}{1 + K_L \cdot \beta(O_3)_{t(U_{max})}} \quad (3)$$

Herein, $q_e$ is the relative occupancy of adsorption sites at pseudo-equilibrium, $q_{max} = f \cdot q_L$ is the adjusted maximum adsorption capacity of the adsorbent (Pt surface of IPMC electrode), $K_L$ is the Langmuir constant related to the affinity of adsorption, and $\beta(O_3)_{t(U_{max})}$ is the pseudo-equilibrium concentration of the adsorbate (dissolved ozone). In the context of this study, the

pseudo-Langmuir model assumes an approximate direct proportionality between the measured sensor voltage and the pseudo-equilibrium occupancy, which is given by the proportionality factor $f$ in the equation above. This formal scale factor accounts for different physical dimensions incorporated into the equation. Under the assumption that $q_e$ approaches the limit of 1, the numerical value of $f$ becomes equal to $q_{max}$ for every individual sensor.

This assumption is supported by the typical cyclic voltammogram of Pt on Nafion as a working electrode in purified water:[68] In the potential range where chemisorption of oxygen adsorbates occurs on the Pt surface (oxygen underpotential deposition), the observed $I(U)$ profile can be approximated by a rectangular graph and thus be interpreted as a capacitor, where the amount of electric charge (given by the anodic current integral in this region) linearly depends on the electrode potential. As the surface coverage of adsorbed oxygen is proportional to the electric charge,[59] the assumption of linear proportionality is justified.

For LOD and LOQ estimation, the noise of the signal baseline was determined to be the limiting characteristic and its standard deviation was quantified to $\sigma_b = 2$ mV, also taking the resolution of the measuring equipment into account. Hence, LOD ($3\,\sigma_b$) and LOQ ($10\,\sigma_b$) correspond to voltages of $\Delta U_{max} = 6$ and $20$ mV, respectively. By solving Equation (3) for $\beta(O_3)_{t(U_{max})}$, Equation (4) is obtained and yields individual concentration values for the different synthesized sensors.

$$\beta(O_3)_{t(U_{max})} = \frac{\Delta U_{max}}{K_L \cdot (q_{max} - \Delta U_{max})} \quad (4)$$

Choosing the most suitable sensor strongly depends on the specific application: If ozone concentrations typically occur in the low µg L$^{-1}$ range (i.e. low LOD values are desired), a steep calibration curve with higher values for $K_L$ is preferred. On the other hand, if a larger dynamic range is required, then sensors with a lower $K_L$ value but higher $q_{max}$ values should be selected.

**Table 4.** Comprehensive overview of the ozone-sensing properties obtained for the sensors listed in Table 3. $AIC_c$ values were calculated for the Freundlich (FR), Langmuir (LA), Redlich–Petersen (RP), and Sips (SI) pseudo-isotherm models. Langmuir pseudo-isotherm regression parameters are given for each sensor as well as the adjusted coefficient of determination ($R^2_{adj.}$) and the limits of detection (LOD) and quantification (LOQ).

| # | $AIC_c$ values | | | | Pseudo–Langmuir fit parameters | | | Analytical parameters | |
|---|---|---|---|---|---|---|---|---|---|
| | FR | LA | RP | SI | $q_{max}$ [mV] | $K_L$ [L mg$^{-1}$] | $R^2_{adj.}$ | LOD [μg L$^{-1}$] | LOQ [μg L$^{-1}$] |
| 1 | 48.8 | 46.8 | 66.7 | 65.8 | 426 | 10.90 | 0.861 | 1.3 | 4.5 |
| 2 | 35.8 | 31.9 | 49.3 | 49.3 | 281 | 2.48 | 0.971 | 8.8 | 30.9 |
| 3 | 40.7 | 35.3 | 55.2 | 53.9 | 290 | 5.53 | 0.974 | 3.8 | 13.4 |
| 4 | 46.9 | 48.1 | 56.8 | 56.8 | 280 | 5.06 | 0.834 | 4.3 | 15.2 |
| 5 | 61.6 | 57.2 | 66.3 | 64.0 | 583 | 7.42 | 0.880 | 1.4 | 4.8 |
| 6 | 52.6 | 52.8 | 58.9 | 58.9 | 357 | 10.03 | 0.890 | 1.7 | 5.9 |
| 7 | 73.4 | 68.4 | 73.9 | 73.8 | 597 | 12.75 | 0.930 | 0.8 | 2.7 |
| 8 | 56.2 | 53.2 | 60.3 | 58.6 | 418 | 2.14 | 0.898 | 6.8 | 23.5 |
| 9 | 43.9 | 43.4 | 34.3 | 30.4 | 1023 | 0.79 | 0.793 | 7.4 | 25.1 |
| 10 | 40.2 | 37.2 | 44.7 | 38.2 | 381 | 1.08 | 0.941 | 14.8 | 51.3 |
| 11 | 66.2 | 68.0 | 70.1 | 70.1 | 454 | 13.58 | 0.881 | 1.0 | 3.4 |
| 12 | 30.8 | 32.8 | 50.6 | 50.8 | 324 | 20.45 | 0.848 | 0.9 | 3.2 |
| 13 | 50.3 | 44.4 | 64.3 | 64.4 | 567 | 19.41 | 0.959 | 0.6 | 1.9 |
| 14 | 53.5 | 44.2 | 50.3 | 49.0 | 722 | 2.34 | 0.967 | 3.6 | 12.2 |
| 15 | 63.5 | 64.9 | 69.4 | 68.9 | 647 | 11.61 | 0.881 | 0.8 | 2.7 |
| 16 | 58.7 | 55.9 | 62.8 | 59.8 | 542 | 7.24 | 0.783 | 1.5 | 5.3 |
| 17 | 48.5 | 48.2 | 56.9 | 56.4 | 351 | 21.82 | 0.891 | 0.8 | 2.8 |
| 18 | 46.3 | 41.4 | 45.5 | 46.2 | 257 | 4.62 | 0.974 | 5.2 | 18.3 |
| 19 | 62.0 | 53.6 | 59.7 | 59.6 | 435 | 12.42 | 0.941 | 1.1 | 3.9 |
| 20 | 49.4 | 48.7 | 67.8 | 67.9 | 561 | 36.05 | 0.872 | 0.3 | 1.0 |
| 21 | 57.7 | 51.2 | 55.0 | 53.6 | 621 | 25.97 | 0.974 | 0.4 | 1.3 |
| 22 | 50.8 | 52.2 | 59.8 | 60.2 | 364 | 13.27 | 0.874 | 1.3 | 4.4 |
| 23 | 63.8 | 60.6 | 66.9 | 66.2 | 572 | 6.71 | 0.899 | 1.6 | 5.4 |
| 24 | 62.8 | 45.2 | 52.0 | 51.8 | 495 | 23.65 | 0.989 | 0.5 | 1.8 |
| 25 | 49.8 | 45.0 | 64.5 | 65.0 | 686 | 10.94 | 0.958 | 0.8 | 2.7 |

An overview of the pseudo-Langmuir regression parameter derived from the sensor response curves as well as resulting LOD and LOQ values are given in Table 4.

For most regressions, an adjusted coefficient of determination $R^2_{adj.} > 0.85$ is achieved, indicating a sufficient description of the data points by the pseudo-Langmuir regression model. The calculated $q_{max}$ values range from 257 to 1023 mV and suggest a notable span in the obtained surface properties as $q_{max}$ represents the upper limit for an observable change in voltage when all binding sites on the sensor surface are occupied by analyte molecules. For the parameter $K_L$, which is linked to the energy of adsorption, values range from 0.79 to 36.05 L mg$^{-1}$ and thus exceed an order of magnitude. This further implies differences concerning the surfaces of the individual sensors as larger $K_L$ values are related to stronger interactions between the adsorbate and adsorbent.[61] However, the obtained values for $q_{max}$ and $K_L$ exhibit a much broader range than expected as the adsorption behavior is primarily a material property of Pt in the presence of ozone. In consequence, while the Langmuir pseudo-isotherm yields the most suitable fit according to the $AIC_c$ criterion, it is

indicated that other models may consider the occurring phenomena more accurately.

Considering all sensors, mean LOD and LOQ values of 2.9 and 9.9 μg L$^{-1}$ are determined, respectively. These limits enable confident monitoring of UPW for the application during pharmaceutical-grade water sanitization.

## 2.4. Evaluation of General Trends between Synthesis Parameters, Physicochemical Properties, and Ozone-Sensing Behavior

The aforementioned findings show that both the physicochemical and ozone-sensing properties are strongly influenced by the selected synthesis conditions. It would therefore be desirable to identify underlying correlations in order to enable tailoring IPMC sensors to their specific application in disinfection monitoring. The accurate calculation of numerical relations from the presented dataset bears challenges as a fractional factorial study design was deliberately chosen to limit high-value resources (e.g. platinum, Nafion). While this approach cannot resolve all
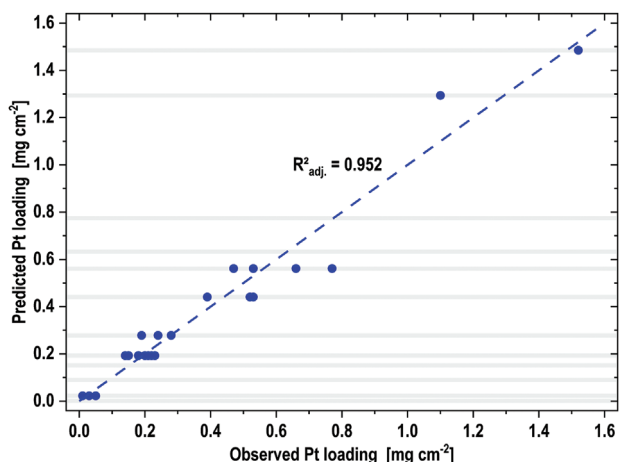
**ADVANCED
SCIENCE NEWS**

www.advancedsciencenews.com

**ADVANCED
MATERIALS
TECHNOLOGIES**

www.advmattechnol.de

**Figure 4.** Plotting the predicted (according to Equation (6)) versus observed values for the regression model of the Pt loading indicates a good model accuracy ($R^2_{adj.} > 0.95$). A step-like profile of the calculated data points arises from the fact that the regression model is based on a limited amount of input parameters and can only assume a defined number of levels for the given dataset (gray horizontal lines).

higher-order interactions due to confounding factors, this can be considered a minor issue, as only a small proportion of all variables exhibit statistically significant effects (effect sparsity principle[69]) and main effects are more likely to be important than two-factor or higher-order interactions (hierarchical ordering principle[70]). Therefore, the study design is justified by allowing the beneficial extraction of general trends from a cost-effective screening of synthesis conditions affecting the physicochemical and sensing properties.

Both the direct correlations between synthesis parameters and sensing properties as well as correlations between physicochemical properties and sensing properties were considered. However, valid models were only established for certain properties, with the best results found for Pt loading, demonstrated in **Figure 4**.

To verify whether all prerequisites for the multiple linear regression analysis are given, both the normal distribution and homoscedasticity of the residuals are evaluated. For the Pt loading a Box–Cox transformation (Equation (5)) of the dataset had to be performed.[71] As a result, only a few data points exhibit large residuals, that is, for a majority of data points there are only minor deviations between the measured values and the modeled data. This can also be seen in Figure 4 as the overall model shows a good agreement between observed and predicted data ($R^2_{adj.} > 0.95$). This is especially remarkable as the refined model merely requires information about the initial Pt concentration, the selected reducing agent, and the applied reduction strategy (Equation (6)). In turn, a reliable prediction of Pt loadings may be used to prepare IPMCs with defined physicochemical properties even beyond sensing applications by employing the presented model.

$$\text{Pt loading}_{trans} = \frac{\left(\text{Pt loading}\right)^{\lambda} - 1}{\lambda} \text{ with } \lambda = 0.545 \quad (5)$$

$$\text{Pt loading}_{trans} = 0.174 + 0.598 \cdot c(\text{Pt})_{init} - 2.391$$

$$\cdot \begin{vmatrix} \text{Red. agent} \\ 1 \text{ for } N_2H_2 \\ 0 \text{ for NaBH}_4, \text{ KBH}_4 \end{vmatrix} - 0.580 \cdot \begin{vmatrix} \text{Red. strategy} \\ 1 \text{ for } 3 \times 20 \text{ min} \\ 0 \text{ for } 1 \times 60 \text{ min} \end{vmatrix} \quad (6)$$

Furthermore, it can be observed that the calculated data points form horizontal lines, resulting in a step-like profile. This is a direct consequence of the underlying regression model consisting of just three input parameters which were varied on only 2 or 3 defined levels for the given dataset. As a result, no more than 12 different levels of Pt loading can be extracted from the regression model. Yet, this degree of differentiation is already sufficient for a reasonable estimation of the metal loading, merely on the basis of given synthesis conditions and without the necessity of performing any measurements on the manufactured products. Other synthesis variables, such as, for example, the concentration of the reducing agent, have shown to be less important as they were not limiting the reduction process and were subsequently not implemented into the refined regression model for Pt loading.

An overview of all successfully established regression models is given in **Figure 5**. Only those models are included that achieved a $p < 0.05$ and $R^2_{adj.} > 0.50$ to ensure sufficient model adequacy and significance for a general estimation of physicochemical or sensing properties. In this context, the $p$-value indicates the probability that the identified correlation was randomly obtained. Just four of all evaluated and refined models fulfill these criteria, the remainder led to insufficient fits or poor significance. In consequence, no significant models were established to describe the expected sensing properties merely based on given synthesis conditions. All obtained regression models are purely based on main effects; two-factor interactions were considered but none were identified as being statistically significant. In general, factors with $p < 0.05$ were typically not included in the model refinement unless explicitly stated. Equations for the remaining regression models are given in Supporting Information.

For the radiographic blackening, a statistically significant and adequate model was obtained. In contrast to the Pt loading regression model, the choice of either $NaBH_4$ or $KBH_4$ shows a statistically significant distinction with respect to the blackening, which is a direct result of different mass attenuation coefficients of remaining cations in the Nafion structure. A rather decent model was also obtained for the Pt layer thickness. With a $p$-value of 0.11, the use of a supporting solution shows a formally insignificant effect, however, omitting this minor factor from the regression has been shown to degrade the quality of the model substantially.

The presented dataset yielded no valid regression models between the synthesis parameters and the sensing properties and therefore does not allow for a direct correlation. Apparent patterns in some Q-Q plots, irrespective of the choice of variables, indicate that there may be further, complex influencing factors that have not been considered so far. In a related context, Sakthivel et al. have previously indicated a relationship between surface morphology and the choice of borohydride salt.[31] However, with $K_L$ (expressing the pseudo-Langmuir curvature), a single structure-property relationship is successfully described by a statistically significant model. Although blackening and Pt
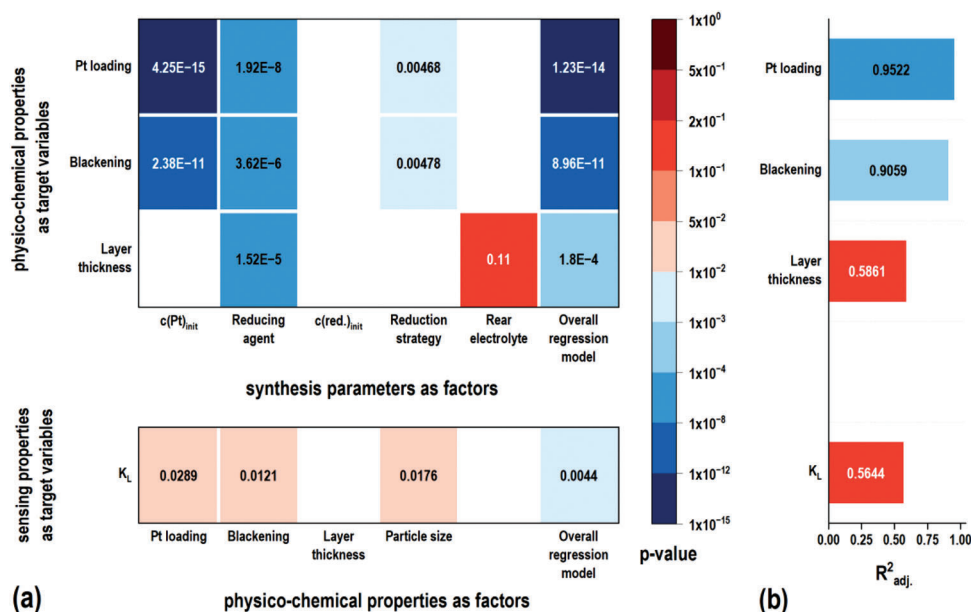
**ADVANCED
SCIENCE NEWS**

www.advancedsciencenews.com

**ADVANCED
MATERIALS
TECHNOLOGIES**

www.advmattechnol.de

**Figure 5.** a) Heatmap of *p*-values for all multiple linear regression models that yielded sufficient model adequacy and significance. The color gradient corresponds to the *p*-values, with blue tiles of varying intensity referring to factors of higher significance ($p < 0.01$). b) Adjusted coefficients of determination for the obtained valid regression models. For Pt loading and blackening $R^2_{adj.} > 0.90$ were achieved.

loading were expected to describe somewhat redundant information, both factors contribute significantly to the model, while layer thickness was excluded during model refinement due to insignificance. Furthermore, particle size is another contributing factor to this model; however, since missing values had to be considered, this resulted in a loss in statistical power due to fewer data points for model refinement. Yet, removing the particle size from the regression model would also lead to lower $R^2_{adj.}$ values.

## 3. Conclusion

In this study, platinum-based IPMCs were synthesized using a simple laboratory-scale setup and characterized with respect to the intended use as potentiometric sensors for the quantification of dissolved ozone in UPW monitoring. Depending on the selected synthesis parameters the obtained sensor materials vary greatly in appearance and feature nanostructured Pt surfaces with particle diameters in the range of 40 to 90 nm. The formation of contiguous Pt layers only occurred when using tetraborohydrides as reducing agents, however, IPMCs prepared with hydrazine also led to sensitive ozone sensors despite possessing low Pt loadings.

As common non-destructive determination methods for the individual metal loading are limited due to gravimetric resolution, a radiographic approach was evaluated and allows for a sufficient estimation of the Pt content. However, for low Pt loadings, other incorporated elements may contribute considerably to the overall X-ray absorption, impairing the accuracy of the method.

Sensor response properties in ozonated water can be conclusively described by Langmuir pseudo-isotherms in the potentiometric measuring setup. Mean LODs of $\approx 3$ µg L$^{-1}$ were enabled, qualifying the materials as suitable sensors in pharmaceutical systems for cold water storage.
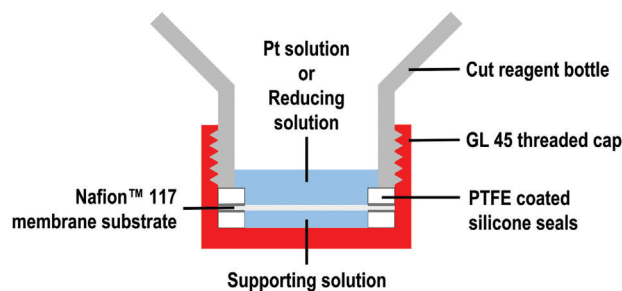


**Figure 6.** Schematic model of the experimental setup: The reagent bottle, its threaded cap, and two sealing discs allow the Nafion membrane to be contacted simultaneously by both the Pt solution or the reducing solution from above and the supporting solution from beneath.

Even from a limited dataset, it is possible to accurately correlate selected physicochemical properties with given synthesis conditions, however, sensing properties did not yield satisfying regression models. An assumed influence by the supporting solution was only identified for the Pt layer thickness. By improving the microscopic analysis of particle sizes, especially for smaller nanoparticles expected when using hydrazine as a reductant, modeling of sensing properties might be achievable at a higher accuracy and significance.

The obtained results contribute to prospective targeted syntheses of cost-effective IPMC sensor materials with defined physicochemical properties and enable miniaturized sensor setups that can be retrofitted at various key spots within UPW storage systems. Future studies can improve by a larger range of different sensors, which would be more feasible with an optimized sensor design to require even fewer resources. Furthermore, the observed sensor response and reset times limit monitoring
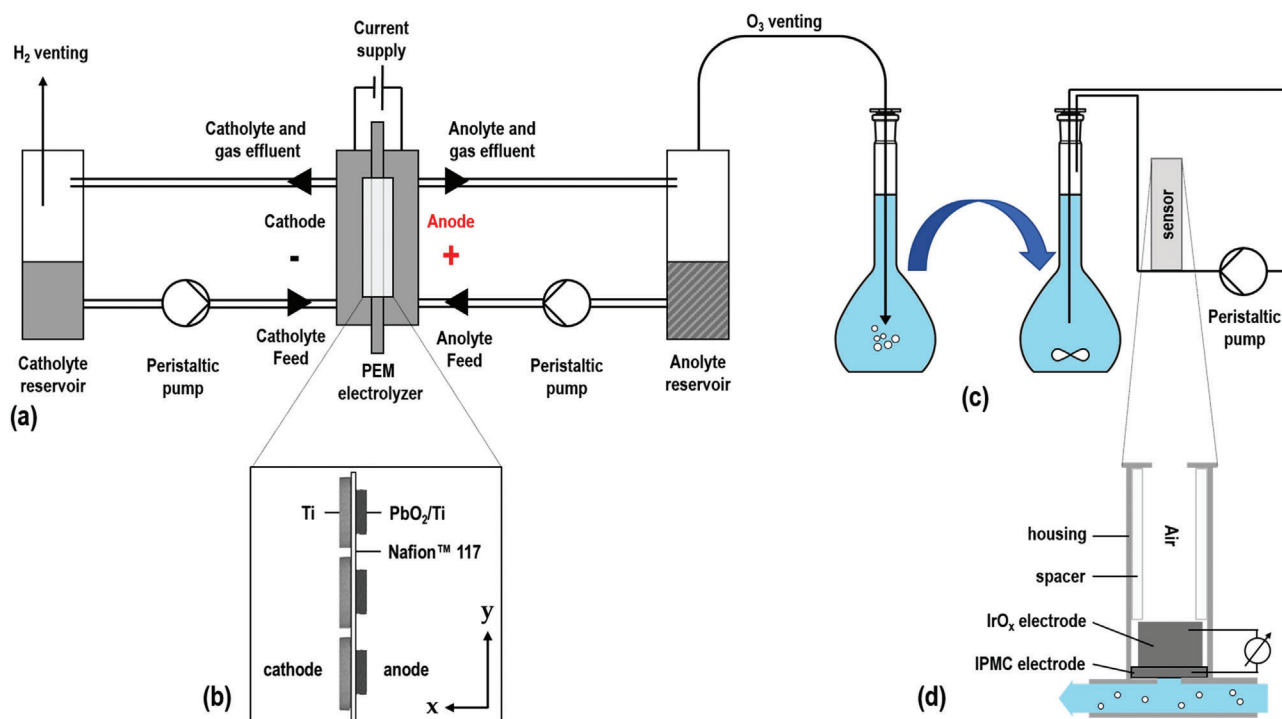
**Figure 7.** Scheme of the experimental setup for a) ozonated water production and b) arrangement of the SMEA. 18.2 MΩ ultrapure water from the reservoir is pumped through both the anodic and cathodic half-cells of the PEM electrolyzer, with oxidants being dissolved into the anaolyte. Gaseous ozone from the analytic cycle is bubbled into a separate ultrapure water reservoir to provide solutions with ozone as the only oxidant present. c) The ozonated water is then pumped along d) a simple sensor setup which allows for quick material exchange.

applications that demand quick response qualities and should gain further attention. A promising approach for this purpose may involve the presence of stabilizing agents during synthesis to better control Pt nanoparticle growth which might also be of interest for further applications of IPMCs.

## 4. Experimental Section

*Preparation of Platinized Nafion Membrane Electrodes via Impregnation-Reduction Method*: Nafion 117 membranes (Chemours, Wilmington, Delaware, USA) were conditioned according to Sakthivel et al.[31] and placed in the apparatus depicted in **Figure 6**. The setup consisted of a GL 45 screw cap, the PEM (circular, $d = 41$ mm) placed between two silicone-PTFE seals (with circular center cut-out, $d = 35$ mm), and a horizontally cut PP reagent bottle. The lower cavity beneath the membrane provided a supporting solution while the funnel-shaped reagent bottle acted as the reservoir for the metal and reducing solutions to which the membranes were exposed during the impregnation-reduction process.

The synthesis followed and expanded the impregnation-reduction methods from the literature.[23,31] All chemicals were in analytical grade quality and all solutions thereof were prepared from 18.2 MΩ UPW. Both UPW, as well as KCl and $K_2SO_4$ (Merck KGaA, Darmstadt, Germany) electrolytes (13 mmol L$^{-1}$), were evaluated as supporting solutions.[40,52]

3 mL of the supporting solution was filled into the cavity before placing the prepared membrane substrate into the setup. Subsequently, a $Pt(NH_3)_4Cl_2$ (Aldrich, St. Louis, MO, USA) solution (10 mL) with defined concentration levels was allowed to impregnate the membrane with Pt for 1 h at room temperature, supported by a 3D platform rotator (Grant Instruments, Shepreth, United Kingdom). Thereafter, the impregnation solution was exchanged for a reducing solution (15 mL), prepared in an aqueous

$NH_3/NH_4^+$ buffer system (100 mmol L$^{-1}$, $pH = 9.25$). Reducing agents and concentrations were varied in a fractional factorial design and include $NaBH_4$, $KBH_4$, and $N_2H_4$ (all VWR Chemicals, Radnor, PA, USA). The reduction treatment was carried out for 1 h under magnetic stirring. All 25 IPMC variations were synthesized as duplicates.

*Structural and Elemental Characterization of the Synthesized Pt Layers*: All characterization steps were performed after prior reloading and drying of the synthesized Pt/Nafion IPMCs. Pt loading values were determined by atomic emission spectroscopy on an ARCOS ICP OES system (Spectro, Kleve, Germany) after digesting circular cut-outs ($d = 6$ mm) in boiling aqua regia (12 mL) for 30 min and subsequent dilution with UPW. ICP OES measurements were carried out as triplicates at 1400 W incident power and an integration time of 12 s after a rinse time of 60 s.

The determination of both thickness, position, and uniformity of the Pt layers was performed using a 7200F field-emission scanning electron microscope (JEOL, Akishima, Japan) at 2 kV acceleration voltage. All samples were degassed and dried in a desiccator for at least 24 h before SEM analysis. The layer thickness was acquired via SEM imaging in a 10-fold determination at the cross-section of the composite material. The particle size was determined at five representative spots on the SEM image of the respective electrode surface using the ImageJ distribution Fiji.[72] In order to enable Pt identification via Pt-M$\alpha$ and Pt-M$\beta$ emission lines, elemental analyses were carried out using a Bruker XFlash 6|60 EDX detector at 15 kV acceleration voltage.

Radiographic assessment of the Pt loading was performed using a Skyscan 1275 computed tomography scanner (Bruker, Billerica, MA, USA) at 15 kV acceleration voltage and 150 µA current with 16-bit image acquisition. Three representative circular sections ($d = 6$ mm) were taken from each radiograph and collected as a 2D color value dataset. Mean values were calculated from the individual pixels using OriginPro 2022 (OriginLab, Northampton, MA, USA) and the gray value of the individual electrodes was determined using the 256 gray levels available in the 8-bit grayscale depth.

**ADVANCED
SCIENCE NEWS**

www.advancedsciencenews.com

**ADVANCED
MATERIALS
TECHNOLOGIES**

www.advmattechnol.de

**Table 5.** Overview of synthesis parameters, physicochemical properties, and sensing parameters evaluated in the present study. LOQ was not included in the multiple linear regression analysis due to linear dependency with LOD.

| Synthesis parameters | Physicochemical properties | Sensing parameters |
|---|---|---|
| Initial Pt concentration | Pt loading | Langmuir fit parameter $q_{max}$ |
| Reducing agent | Radiographic blackening | Langmuir fit parameter $K_L$ |
| Initial reductant concentration | Layer thickness | Coefficient of determination $R^2_{adj.}$ |
| Reduction strategy | Particle size | Limit of detection LOD |
| Supporting solution | | Limit of quantification LOQ |

*Characterization of Ozone Sensing Properties*: To prepare aqueous solutions with defined ozone content, the setup depicted in **Figure 7** is used for all experiments. A structured membrane-electrode assembly (SMEA), consisting of a Nafion 117 membrane and seven pairs of $PbO_2$-coated porous titanium anodes and porous titanium cathodes (all Innovatec Gerätetechnik GmbH, Rheinbach, Germany), was mounted within a PVC housing (as previously described in ref. [73]). The ozone-rich gas phase of the anodic half-cell was exhausted into a separate flask to prevent the introduction and subsequent measurement of other electrochemically formed oxygen species.

Subsequently, the ozonated water was stirred gently and pumped along the sensor setup shown in Figure 7d, containing one IPMC specimen per experiment (representing each synthesis condition), a PTFE spacer, and an $IrO_x$ electrode (De Nora, Milan, Italy) assembled within a sealed housing. No additional reference electrode had to be incorporated as there is no current flow during the potentiometric measurement which would lead to a polarization of the $IrO_x$ electrode. Furthermore, $IrO_x$ has proven to provide a stable electrode potential ($E \approx 880$ mV vs SHE) while the surrounding media exhibit constant pH values.[74–76] As Nafion fulfills this requirement under ultrapure water conditions, a stable reference electrode is thus guaranteed.[77,78]

For sensor characterization experiments, the UPW used for sensor conditioning was replaced by ozonated ultrapure water with a target concentration range of $\approx 10$ μg $L^{-1}$ to 1.0 mg $L^{-1}$. Sensor signals were acquired by measuring the potential between the Nafion-supported Pt surface (exposed to the ozonated water) and the $IrO_x$ surface (exposed to ambient air). In order to allow for a justified extraction of regression parameters from the signal response properties, signals were collected for at least 5 different ozone concentrations.

At the same as the sensor was initially supplied with a new concentration level of ozonated water, the ozone content of the solution was quantified colorimetrically for an off-line sample via the DPD method in accordance with DIN 38408-3:2011-04, using KI, $KIO_3$, $Na_2HPO_4$, $KH_2PO_4$, $Na_2S_2O_3$, $H_2SO_4$, starch (all p.a. grade, Carl Roth, Karlsruhe, Germany), and DPD (N,N-diethyl-p-phenylenediamine sulfate; Merck, Burlington, MA, USA) on a DR6000 spectral photometer (Hach Lange, Düsseldorf, Germany). On a daily basis, the required $I_2$ solutions (2.5 mmol $L^{-1}$) were freshly prepared and checked for their titers with a $Na_2S_2O_3$ solution (10 mmol $L^{-1}$) using $KIO_3$ and KI as primary standards. The same procedure is used for the characterization of ozone decay within the setup displayed in Figure 7c.

*Model Development and Statistical Analysis*: Additional statistical evaluations were performed using the free software environment R for statistical computing,[79] supported by the *MASS* package,[80] in order to identify general trends between all groups of parameters measured and evaluated in the present study (see **Table 5**). A multiple linear regression analysis was chosen to estimate the magnitude and direction of selected factor effects by regressing the physicochemical properties and the sensing parameters with the synthesis conditions of the sensor materials. To integrate categorical variables in the regression models, dummy variables were used.

Due to the fractional factorial study design, not all factor interactions were considered; instead, higher-order interactions of three or more parameters were excluded as they can be considered less probable (hierarchical ordering principle).[81] Furthermore, only selected two-factor interactions were evaluated, for which a cause-effect relationship was considered plausible.

Initial regression models that included all factors and assumed interactions were set up and refined. The developed reduced models only included statistically significant contributing factors, which were identified by analysis of variance. The model adequacy was verified with normal probability and residual plots, and a Box–Cox transformation was performed where applicable.[71]

## Supporting Information

Supporting Information is available from the Wiley Online Library or from the author.

## Acknowledgements

## Conflict of Interest

One of the authors, Samuel Stucki, works as scientific consultant for Innovatec Gerätetechnik GmbH which provided resources for the present study. All other authors declare no conflict of interest.

## Data Availability Statement

The data that support the findings of this study are available from the corresponding author upon reasonable request.

## Keywords

**2202043 (11 of 13)**

[1] United States Pharmacopoeia, Water for Pharmaceutical Purposes <1231>, USP 40 – NF35, **2017**.

[2] European Pharmacopeia, 9th Edition, **2017**, p. 5790–5791.

[3] X. Zhang, Y. Yang, H. H. Ngo, W. Guo, H. Wen, X. Wang, J. Zhang, T. Long, *Sci. Total Environ.* **2021**, *785*, 147254.

[4] Y. Choi, Y. june Choi, *Water Res.* **2010**, *44*, 115.

[5] M. Bourgin, E. Borowska, J. Helbing, J. Hollender, H. P. Kaiser, C. Kienle, C. S. McArdell, E. Simon, U. von Gunten, *Water Res.* **2017**, *122*, 234.

[6] M. Fabbricino, L. D'Antonio, *Environ. Technol.* **2012**, *33*, 539.

[7] W. Ding, S. Cao, W. Jin, X. Zhou, C. Wang, Q. Jiang, H. Huang, R. Tu, S.-F. Han, Q. Wang, *Water Res.* **2019**, *160*, 339.

[8] S. Stucki, D. Schulze, D. Schuster, C. Stark, *Pharm. Eng.* **2005**, *25*, 40.

[9] M. Florjanič, J. Kristl, *Drug Dev. Ind. Pharm.* **2006**, *32*, 1113.

[10] T. Wang, D. A. Reckhow, *Ozone: Sci. Eng.* **2016**, *38*, 373.

[11] H. Taube, *Trans. Faraday Soc.* **1957**, *53*, 656.

[12] J. Hoigné, H. Bader, W. R. Haag, J. Staehelin, *Water Res.* **1985**, *19*, 993.

[13] W. Gottardi, *Fresenius' J. Anal. Chem.* **1998**, *362*, 263.

[14] M. L. Kilpatrick, C. C. Herrick, M. Kilpatrick, *J. Am. Chem. Soc.* **1956**, *78*, 1784.

[15] S. Uchiyama, T. Ikarugi, M. Mori, K. Kasama, Y. Ishikawa, M. Kaneko, A. Umezawa, *Electroanalysis* **1993**, *5*, 121.

[16] J. H. Stanley, J. D. Johnson, *Anal. Chem.* **1979**, *51*, 2144.

[17] R. B. Smart, R. Dormond-Herrera, K. H. Mancy, *Anal. Chem.* **1979**, *51*, 2315.

[18] Y. Einaga, I. Tribidasarianggraningrum, Y. Ishii, S. Sekiguchi, K. Murata, US9625405B2, **2017**.

[19] Y. Ishii, T. A. Ivandini, K. Murata, Y. Einaga, *Anal. Chem.* **2013**, *85*, 4284.

[20] K. Vandersmissen, F. De Smedt, C. Vinckier, *Ozone: Sci. Eng.* **2008**, *30*, 300.

[21] H. Takenaka, E. Torikai, Y. Kawami, N. Wakabayashi, *Int. J. Hydrogen Energy* **1982**, *7*, 397.

[22] S. D. Thompson, L. R. Jordan, M. Forsyth, *Electrochim. Acta* **2001**, *46*, 1657.

[23] P. S. Fedkiw, *J. Electrochem. Soc.* **1989**, *136*, 899.

[24] M. Rashid, T.-S. Jun, Y. S. Kim, *J. Nanosci. Nanotechnol.* **2013**, *13*, 3627.

[25] M. Sakthivel, W. Weppner, *J. Solid State Electrochem.* **2007**, *11*, 561.

[26] Y. Ming, Y. Yang, R. P. Fu, C. Lu, L. Zhao, Y. M. Hu, C. Li, Y. X. Wu, H. Liu, W. Chen, *Adv. Mater. Technol.* **2018**, *3*, 1800257.

[27] S. Biswas, Y. Visell, *Adv. Mater. Technol.* **2019**, *4*, 1900042.

[28] M. Parrilla, R. Cánovas, F. J. Andrade, *Electroanalysis* **2017**, *29*, 223.

[29] C. Ramesh, N. Murugesan, M. V. Krishnaiah, V. Ganesan, G. Periaswami, *J. Solid State Electrochem.* **2008**, *12*, 1109.

[30] Y. Tanaka, S. Uchinashi, Y. Saihara, K. Kikuchi, T. Okaya, Z. Ogumi, *Electrochim. Acta* **2003**, *48*, 4013.

[31] M. Sakthivel, W. Weppner, *Sensors* **2006**, *6*, 284.

[32] Y. C. Weng, K. C. Hung, *Sens. Actuators, B* **2009**, *141*, 161.

[33] L. Xie, J. Lu, H. Yan, *Electroanalysis* **1998**, *10*, 842.

[34] R. Knake, P. C. Hauser, *Anal. Chim. Acta* **2002**, *459*, 199.

[35] G. Schiavon, G. Zotti, G. Bontempelli, *Anal. Chem.* **1990**, *62*, 293.

[36] T.. Chou, K.. Ng, S.. Wang, *Sens. Actuators, B* **2000**, *66*, 184.

[37] X. Z. Yuan, S. Zhang, J. C. Sun, H. Wang, *J. Power Sources* **2011**, *196*, 9097.

[38] Y. M. Obeidat, A. J. Evans, W. Tedjo, A. J. Chicco, E. Carnevale, T. W. Chen, *Sens. Actuators, B* **2018**, *276*, 72.

[39] T. Yin, W. Qin, *TrAC, Trends Anal. Chem.* **2013**, *51*, 79.

[40] N. J. C. Ingle, A. Sode, I. Martens, E. Gyenge, D. P. Wilkinson, D. Bizzotto, *Langmuir* **2014**, *30*, 1871.

[41] R. Liu, *J. Electrochem. Soc.* **1992**, *139*, 15.

[42] P. Hosseinabadi, M. Javanbakht, L. Naji, H. Ghafarian-Zahmatkesh, *Ind. Eng. Chem. Res.* **2018**, *57*, 434.

[43] A. Sode, N. J. C. Ingle, M. McCormick, D. Bizzotto, E. Gyenge, S. Ye, S. Knights, D. P. Wilkinson, *J. Membr. Sci.* **2011**, *376*, 162.

[44] J. Zhao, C. Huang, S. Zhang, F. Qu, R. Wang, H. Jiang, M. Yang, *Sens. Actuators, B* **2021**, *341*, 129993.

[45] B. L. Cushing, V. L. Kolesnichenko, C. J. O'Connor, *Chem. Rev.* **2004**, *104*, 3893.

[46] L. Daniel, A. Bonakdarpour, D. P. Wilkinson, *J. Power Sources* **2020**, *471*, 228418.

[47] P. C. Lee, T. H. Han, D. O. Kim, J. H. Lee, S. J. Kang, C. H. Chung, Y. Lee, S. M. Cho, H. G. Choi, T. Kim, E. Lee, J. Do Nam, *J. Membr. Sci.* **2008**, *322*, 441.

[48] P. C. Lee, J. E. Hyun, S. K. Jeoung, J. Do Nam, T. Hwang, K. J. Kim, K. C. Solasa, *Smart Mater. Struct.* **2019**, *28*, 054003.

[49] P. Millet, M. Pineri, R. Durand, *J. Appl. Electrochem.* **1989**, *19*, 162.

[50] D. G. Bessarabov, W. Michaels, R. D. Sanderson, *J. Membr. Sci.* **2000**, *179*, 221.

[51] H. Ito, T. Maeda, A. Nakano, H. Takenaka, *Int. J. Hydrogen Energy* **2011**, *36*, 10527.

[52] L. Daniel, A. Bonakdarpour, D. P. Wilkinson, *ACS Appl. Nano Mater.* **2019**, *2*, 3127.

[53] S. Dadashi, R. Poursalehi, H. H. Delavari, *Comput. Methods Biomech. Biomed. Eng.: Imaging Visualization* **2019**, *7*, 420.

[54] O. Rabin, J. M. Perez, J. Grimm, G. Wojtkiewicz, R. Weissleder, *Nat. Mater.* **2006**, *5*, 118.

[55] D. Gardoni, A. Vailati, R. Canziani, *Ozone: Sci. Eng.* **2012**, *34*, 233.

[56] J. Staehelin, J. Holgné, *Environ. Sci. Technol.* **1982**, *16*, 676.

[57] J. L. Sotelo, F. J. Beltran, F. J. Benitez, J. Beltran-heredia, *Ind. Eng. Chem. Res.* **1987**, *26*, 39.

[58] N. A. Saliba, Y. L. Tsai, C. Panja, B. E. Koel, *Surf. Sci.* **1999**, *419*, 79.

[59] H. Angerstein-Kozlowska, B. E. Conway, W. B. A. Sharp, *Chem* **1973**, *43*, 9.

[60] H. Freundlich, *Z. Phys. Chem.* **1907**, *57U*, 385.

[61] I. Langmuir, *J. Franklin Inst.* **1917**, *184*, 721.

[62] K. P. Burnham, D. R. Anderson, *Wildl. Res.* **2001**, *28*, 111.

[63] E. J. Wagenmakers, S. Farrell, *Psychon. Bull. Rev.* **2004**, *11*, 192.

[64] O. Redlich, D. L. Peterson, *J. Phys. Chem.* **1959**, *63*, 1024.

[65] R. Gutiérrez-Climente, A. Gómez-Caballero, N. Unceta, M. Aránzazu Goicolea, R. J. Barrio, *Electrochim. Acta* **2016**, *196*, 496.

[66] R. Sips, *J. Chem. Phys.* **1948**, *16*, 490.

[67] G. K. Rajahmundry, C. Garlapati, P. S. Kumar, R. S. Alwi, D. V. N. Vo, *Chemosphere* **2021**, *276*, 130176.

[68] Q. Wang, C. S. Cha, J. Lu, L. Zhuang, *Phys. Chem. Chem. Phys.* **2009**, *11*, 679.

[69] G. E. P. Box, R. D. Meyer, *Technometrics* **1986**, *28*, 11.

[70] C. J. Wu, M. S. Hamada, *Experiments: Planning, Analysis, and Optimization*, John Wiley & Sons, Hoboken, NJ **2011**.

[71] G. E. P. Box, D. R. Cox, *J. R. Stat. Soc., Ser. B* **1964**, *26*, 211.

[72] J. Schindelin, I. Arganda-Carreras, E. Frise, V. Kaynig, M. Longair, T. Pietzsch, S. Preibisch, C. Rueden, S. Saalfeld, B. Schmid, J. Y. Tinevez, D. J. White, V. Hartenstein, K. Eliceiri, P. Tomancak, A. Cardona, *Nat. Methods* **2012**, *9*, 676.

[73] R. Grimmig, P. Gillemot, S. Stucki, K. Günther, H. Baltruschat, S. Witzleben, *Sep. Purif. Technol.* **2022**, *292*, 121063.

[74] O. C. Keller, J. Buffle, *Anal. Chem.* **2000**, *72*, 936.

**ADVANCED
SCIENCE NEWS**

www.advancedsciencenews.com

**ADVANCED
MATERIALS
TECHNOLOGIES**

www.advmattechnol.de

[75] H. Yang, S. K. Kang, C. A. Choi, H. Kim, D. H. Shin, Y. S. Kim, Y. T. Kim, *Lab Chip* **2004**, *4*, 42.

[76] S. Yao, M. Wang, M. Madou, *J. Electrochem. Soc.* **2001**, *148*, H29.

[77] M. Wang, S. Yao, M. Madou, *Sens. Actuators, B* **2002**, *81*, 313.

[78] Z. Zhu, X. Liu, Z. Ye, J. Zhang, F. Cao, J. Zhang, *Sens. Actuators, B* **2018**, *255*, 1974.

[79] R Core Team, *R: A language and environment for statistical computing. R Foundation for Statistical Computing* Vienna, Austria **2020**, https://www.R-project.org/.

[80] B. D. Ripley, W. N. Venables, *Modern Applied Statistics with S*, Springer, New York **2002**.

[81] D. C. Montgomery, *Design and Analysis of Experiments*, John Wiley & Sons, Hoboken, NJ **2017**.